



Deposited via The University of Sheffield.

White Rose Research Online URL for this paper:

<https://eprints.whiterose.ac.uk/id/eprint/215703/>

Version: Published Version

Article:

Poyraz, O. (2023) Influence of build direction and post processes on the material and part attributes of hard resins fabricated by photopolymerization based additive manufacturing. *Materials Research*, 26. e20220362. ISSN: 1516-1439

<https://doi.org/10.1590/1980-5373-mr-2022-0362>

Reuse

This article is distributed under the terms of the Creative Commons Attribution (CC BY) licence. This licence allows you to distribute, remix, tweak, and build upon the work, even commercially, as long as you credit the authors for the original work. More information and the full terms of the licence here:

<https://creativecommons.org/licenses/>

Takedown

If you consider content in White Rose Research Online to be in breach of UK law, please notify us by emailing eprints@whiterose.ac.uk including the URL of the record and the reason for the withdrawal request.

Influence of Build Direction and Post Processes on the Material and Part Attributes of Hard Resins Fabricated by Photopolymerization Based Additive Manufacturing

Ozgur Poyraz^{a*} 

^aEskisehir Technical University, Department of Mechanical Engineering, Eskisehir, Turkiye.

Received: August 12, 2022; Revised: December 30, 2022; Accepted: March 01, 2023

This study aims to contribute to the scientific knowledge by investigating the influence of build direction and post-curing on the material and part attributes of acrylonitrile butadiene styrene (ABS-like) like resins by photopolymerization based additive manufacturing (AM). Specimens were manufactured in different build directions with the parameters that offer the highest density. Two groups of specimens, one as-built and the other post-cured, were subjected to dimensional inspections, surface characterization, fourier-transform infrared spectroscopy (FTIR), thermogravimetric analysis (TGA), hardness measurements, tensile tests, bending tests, Charpy impact tests and the obtained values were reported and benchmarked. It has been observed that the change in the build direction significantly affects the surface roughness and the average surface roughness of the samples produced in the vertical plane is much higher than those produced in the horizontal plane. It was demonstrated that post-curing has a negligible effect on part dimensions and density. It increases hardness, tensile modulus and flexural modulus while reducing elongation and impact resistance. The effects of post-curing on chemical and thermal properties were also compared and it was determined that it improves the thermal stability. In the absence of post-curing, vertical as-built specimens were observed to have higher strength than their horizontal counterparts.

Keywords: *additive manufacturing, vat photopolymerization, post-curing, mechanical testing, surface roughness, thermal characterization.*

1. Introduction

Additive manufacturing (AM), whose development process has accelerated since the beginning of the new millennium, has changed the perspective of both academic researchers and industrial experts on product development, design and manufacturing processes. AM, which has the ability to produce the final products in layers or units stacked on top of each other without the need for tools, fixtures, molds, cores and similar auxiliary devices, has increased the freedom of design with the utilization of these advantages. In addition to its design and production advantages, AM offers suitable options for different materials according to the process group, and today metal, polymer, ceramic and composite materials can be produced via various AM technologies¹.

According to the international standard organizations, AM technologies are classified in seven groups². These are Binder jetting (BJ), Directed energy deposition (DED), Material extrusion (ME), Material jetting (MJ), Powder bed fusion (PBF), Sheet lamination (SL) and VAT photopolymerization (VP)³.

VP technologies are perhaps one of the oldest developed among these seven main groups, and although it could not be commercialized in its early development years, it is the first method to be documented through patents⁴. VP technologies, which are mostly preferred for polymeric materials, employ the principle of deploying ultraviolet (UV) lights to liquid light-curable resins and forming chains between molecules, in

order to generate a solid layer⁵. After the UV light is exposed to the liquid resin, it initiates the polymerization reaction with the help of photoinitiators, and polymer chains are formed between monomers and/or oligomers. Figure 1 shows photopolymerization schematics together with monomers, oligomers and photoinitiators⁵.

While the mentioned method is called Digital Light Processing (DLP) in the application of UV light with the help of projectors, it can be called Continuous Digital Light Processing (CDLP) when this process is done uninterruptedly by means of Light Emitting Diodes (LED). In the CDLP technique, an oxygen-permeable glass can be used instead of normal glass, and by means of the flow directed to a very thin area, the complete adhesion of the cured resin to the glass is prevented. In this way, the risk of deterioration that may occur during the separation of the part is reduced.

The CDLP method is also referred by the term Liquid Crystal Display (LCD), since LED type light sources are located in arrays of liquid crystal display panels. In both DLP and CDLP techniques, the photopolymer is contained in a tank, and the upside-down part is lifted by one-layer thickness after each layer has been exposed to the light. This cycle is repeated until the manufacturing process is completed. Figure 2⁶ shows the schematics of generic VP systems .

Photopolymeric materials which are used in VP are classified under several groups such as standard resins, structural resins, tough (or durable) resins, flexible (or

*e-mail: ozgurpoyraz@eskisehir.edu.tr

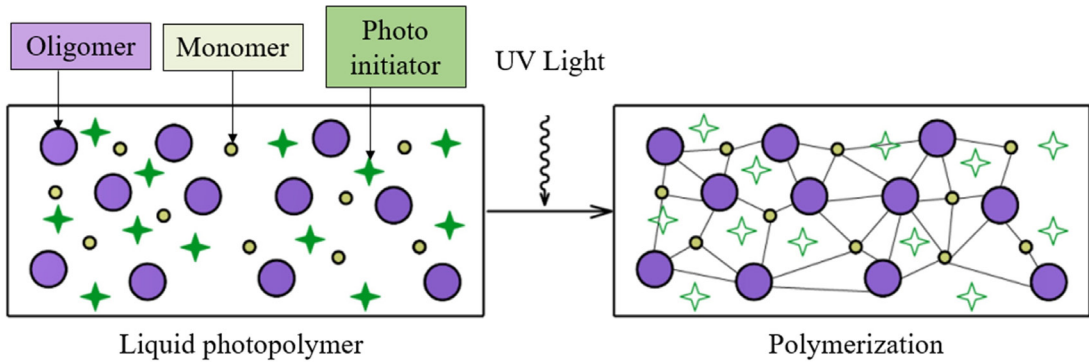


Figure 1. Photopolymerization schematics⁵ (Licensed under CC 4.0).

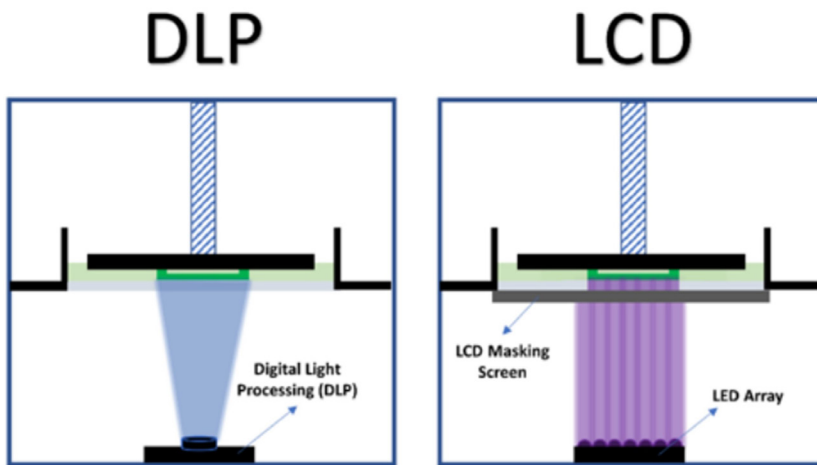


Figure 2. Schematics of generic VP systems⁶ (Licensed under CC 4.0).

elastic) resins, castable resins and biocompatible resins⁷. Although these terms are not technical standards and may differ according to resin material producers, some of them are common and used widely. As the name suggests, tough resins exhibit good example for widely accepted naming and they are employed for the manufacturing of load-bearing products, and their attributes are enhanced through developed formulations which incorporates spiroacetal molecules into the polymer⁸. Among the other classification types, the names of the important compounds that resin contain can be used instead of the character exhibited by the material. Acrylate-based resins are such examples and they can be employed for fast building rates thanks to high reactivities they present^{9,10}. Furthermore, it is reported that the increase in monomer to crosslinker ratios improves mechanical strength as well as resistance against several organic solvents^{10,11}.

Acrylonitrile butadiene styrene (ABS) or ABS-like materials are one of the most common materials employed for polymer products and they can be manufactured via VP, PBF, ME, and MJ based AM techniques as well as conventional methods such as injection molding^{12,13}. When ABS-like materials are applied in VP-based AM techniques, their tensile strengths vary between 39MPa-60MPa while

their elasticity modulus varies between 0.7GPa-2.2GPa. These values are promising when compared to 26MPa-30MPa tensile strength in ME based additive manufacturing, which is not better in terms of surface quality, or MJ based additive manufacturing with higher investment costs^{13,14}. Still, it is important to highlight that the manufacturing strategy, processing parameters and even test conditions play a significant role on the results^{15,16}. Among these the effect of build direction on the product integrity is rarely studied and the few scholarly publications in the literature focuses on general features rather than mechanical strength¹⁶.

This document represents a systematical study on the material and part attributes of ABS-like resins fabricated by VP-based AM. Within the scope of this study, first of all, the initial process and post-curing parameters, in which the highest density is obtained, were determined, and then, using the mentioned parameters, three types of specimens were produced in two sets in two directions. One of the sets, was subjected to the post-curing process. Dimensional measurements, surface roughness characterization, chemical-thermal analyses, hardness, tensile, bending and impact toughness tests were performed with the specimens that were manufactured, and the obtained values were reported and

benchmarked. The data obtained as a result of the research are presented in the following sections of the article.

2. Materials and Methods

During the preliminary studies before this article, density measurements were performed after VP based AM production, post-curing and cleaning operations, and the parameters giving the highest density were determined for both VP based AM and post-curing processes. Then, specimens with geometry suitable for different test and analysis methods were produced, and the dimensions and surface qualities of the specimens were measured. Afterwards, suitable specimens were subjected to Fourier Transform Infrared Spectroscopy (FTIR), Thermogravimetric Analysis (TGA) and Differential Scanning Calorimetry (DSC) analyzes in both raw resin, as-built and post-cured forms, when necessary. The specimens, which were produced with the process parameters determined at the beginning, were also subjected to tests in order to better understand their mechanical behavior. Within the scope of mechanical evaluations, Shore D Hardness, 3-Point Bending and Impact Toughness methods were also used in addition to Tensile Tests. Finally, the fracture surfaces of the specimens, which were subjected to mechanical tests, were examined with a microscope and the results obtained for the whole study were discussed in comparison with the previous literature. Figure 3 shows the cycle of manufacturing, testing and analysis methods applied in this article.

2.1. Material and Specimens

The material used in this study is Alias model fast and hard (ABS-like) resin¹⁷. The transparent resin has a viscosity of 550cP (centipoise) at 25°C.

Three different geometries were used for the tests and analyzes carried out within the scope of this study. Specimen A was used for density measurements, Shore D hardness tests, FTIR analysis and TGA analysis. Specimen B was

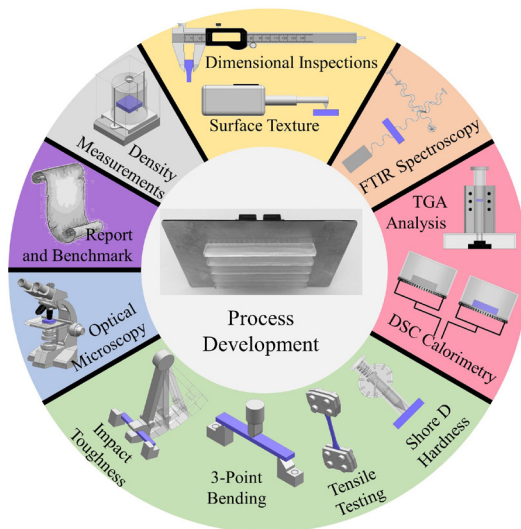


Figure 3. Cycle of manufacturing, testing and analysis methods in this article.

used for tensile tests and microstructural investigations following to tensile tests. Specimen C was used for 3-point bending tests and impact toughness tests. The geometries and dimensions of the specimens produced within the scope of this study and used for the specified tests and analyzes are given in Figure 4.

2.2. Manufacturing

VP-based AM of specimens were performed on a CREALITY LD-002R 3D Printer having a build volume of 119mmx65mmx160mm and equipped with a Ultra HD 2K LCD screen. The job files for the manufacturing were prepared with ChiTuBox slicer software and 2 build layouts were selected as XY and XZ planes. Since the minimum required specimen size according to the tensile test standard did not fit within the limits of the machine in the Y-axis direction, the specimen was not produced in the YZ plane. For the same reason, the longitudinal axis of the specimens produced in the XY and XZ planes was chosen parallel to the machine X-axis direction. On the other hand, the reason why the orientation of the samples produced in the XZ plane is not chosen parallel to the machine Z-axis is that the thickness and length aspect ratio of the specimens is 1:30, and there are risks for achieving the required dimensional accuracy in the slender geometries produced with this level of aspect ratio. As example, the layout of the tensile specimen in the XY and XZ planes are shown in Figure 5.

Layer thickness was maintained at 0.05mm while the exposure time was kept as 10s. Furthermore, auxiliary parameters such as bottom layer count bottom, exposure time, bottom retract height, etc. were also maintained to reach the predefined optimum density of 1.207g/cm³ for the as-built parts as per ISO 11183-1. After the production, the samples were taken to Crealiti Wash and Cure Station UW-01 system, cleaned in isopropyl alcohol with 99.9% purity with the help of a stirring fan, and then 1 set of specimens from each specimen type was post-cured with 36W UV for 10 minutes. All samples were stored in black, opaque sample bags so that both as-built and post-cured specimens would not continue to cure in sunlight or other ambient light sources. Full list of process parameters is given in Table 1.

A total of 18 Specimen A geometries were produced. These were used separately to investigate as-built and

Table 1. Full list of process parameters.

| Parameter | Unit | Value |
|------------------------|--------|-------|
| Layer thickness | mm | 0.05 |
| Bottom layer count | - | 4 |
| Exposure time | s | 10 |
| Bottom exposure time | s | 50 |
| Light-off delay | s | 2 |
| Bottom light-off delay | s | 2 |
| Lift distance | mm | 6 |
| Bottom lift distance | mm | 6 |
| Lifting speed | mm/min | 65 |
| Retract speed | mm/min | 150 |
| Post-Curing time | min | 10 |

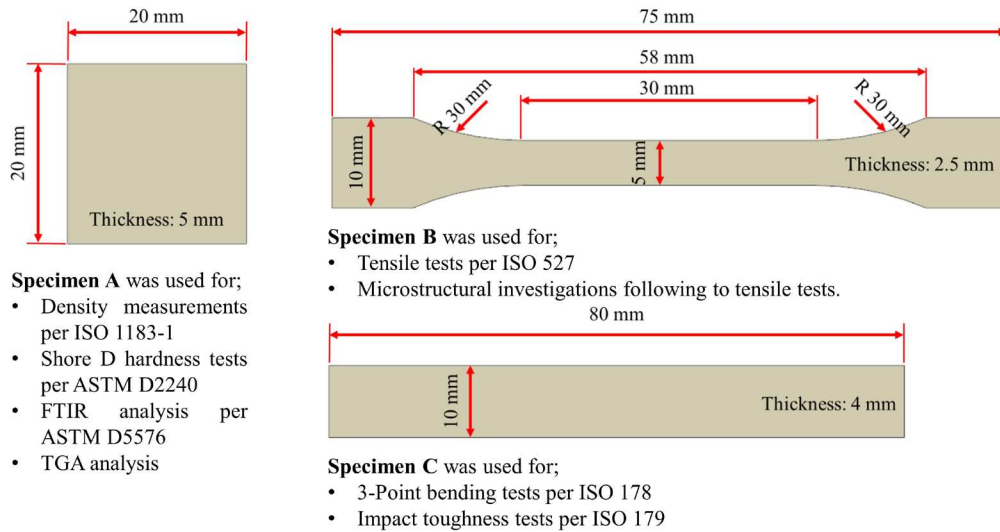


Figure 4. Geometries and dimensions of the specimens.

post-cured conditions in each test and analysis, including density, hardness, FTIR, TGA, and DSC. Among these, density and hardness tests were carried out with 3 repetitions and the specimen quantities of these tests were determined accordingly.

In addition to Specimen A, 12 Specimen B geometries were also produced. 6 of each specimen type were produced to make 3 tests for as-built and post-cured conditions. Processing time for 2 tensile specimens parallel to XY plane was 17 minutes and 56 seconds. Since 6 specimens were produced at 3 set-ups, the total time for tensile specimens parallel to XY plane was 53 minutes and 48 seconds. The tensile specimens parallel to XZ plane could be nested to have 6 parts at one set-up leading a total processing time of 1 hour 3 minutes and 47 seconds. Production of all 24 bending and toughness specimens (Specimen C) took 216 minutes and 28 seconds.

2.3. Dimensional measurement and surface quality

Measurements were carried out both to see the effect of the process parameters used in terms of the product and to ensure that the mechanical performance of the samples did not decrease due to surface defects.

For dimensional measurements, Starrett brand caliper that can measure inside/outside was used. Before the measurements, the accuracy of the caliper was checked with a 20mm diameter calibration pin made by grinding carbide material. The quantities controlled in the measurements include the length, width and thickness of the hardness specimens.

Hexagon Metrology, Tesa Technology RUGOSURF 20 model surface roughness tester was used for surface quality measurements. The reports of the surface quality meter, which is controlled over the computer with the mini USB connection, were obtained from the Measurement Studio software. In measurements made with a tip suitable for surfaces with a curvature of more than 10 mm, contact with the surface was ensured at an angle of approximately 90° and support

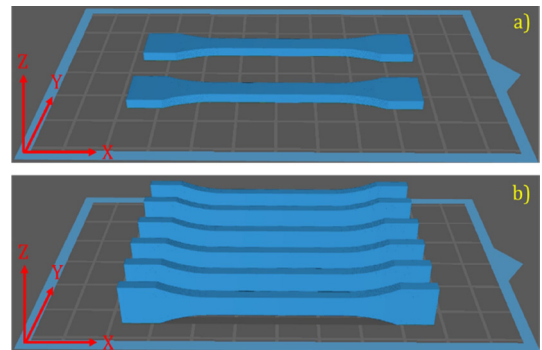


Figure 5. Sample layout of the tensile specimen in the a) XY plane, b) XZ plane.

Table 2. Surface roughness measurement parameters.

| Parameter | Unit | Value |
|---------------------------|---------------|----------|
| Measurement standard | - | ISO 4287 |
| Sampling length (cut-off) | mm | 0.8 |
| Traverse length | mm | 4.8 |
| Reporting output | μm | Ra |

was obtained through positioning bracket when necessary. In the surface roughness measurements, areas that may be risky in terms of reach and contact with the measuring probe were determined, and accordingly, measurements on the risky surfaces along 2.5mm thickness magnitude were avoided. Instead, surface roughness measurements were applied on large surfaces of the samples and scans were completed in two axes parallel to and perpendicular to the tensile direction. Figure 6 shows the surface roughness measuring directions and the measurement process. In addition, the parameters used in surface roughness measurements are given in Table 2.

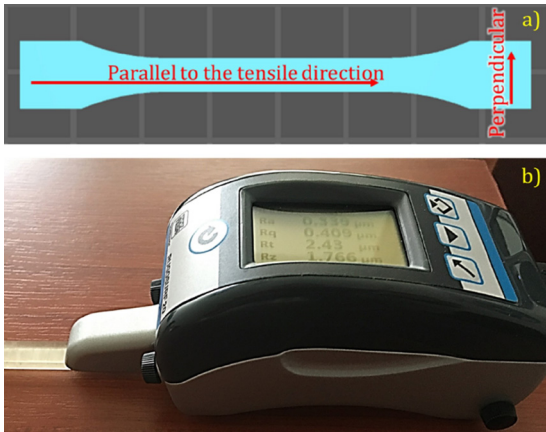


Figure 6. a) Surface roughness measuring directions, b) measurement process.

2.4. Chemical and thermal characterization

Fourier Transform Infrared Spectroscopy (FTIR) technique was chosen to understand the chemical states of the materials and specimens used in the study, and the analyzes were performed on the Thermo Scientific™ Nicolet™ iS50 FTIR spectrometer. Both unprocessed raw resin, as-built specimens and post-cured specimens were subjected to FTIR analysis. Analyzes were performed with 16 scans, 4cm^{-1} resolution, $600\text{--}4000\text{cm}^{-1}$ wavenumber range and diamond crystal.

The method determined for the first step of the thermal characterization was Thermogravimetric Analysis (TGA) and it was performed using the PerkinElmer STA8000 simultaneous thermal analyzer. The initial specimen mass was 6.005mg and the analysis temperature range was $25^{\circ}\text{C}\text{--}1025^{\circ}\text{C}$. Nitrogen was used at 20ml/min mass flow rate in the process where the heating rate was 10°C/min .

Differential Scanning Calorimetry (DSC) analyzes were also conducted on the same analyzer with the same heating and mass flow rate. Based on the previous literature in DSC analysis, the highest temperature was selected as 200°C .

2.5. Mechanical testing

The hardness tests were carried out per ASTM D2240 to determine the Shore D magnitude and the measurements were taken 5 times from each surface in the AMITTARI-AS-120A model test system at 23°C temperature and 10% humidity.

Tensile tests were performed using a Testform AS1 testing system per ISO 527 for a total of 12 times with the specimens produced parallel to XY plane, parallel to XZ plane, as-built and post-cured. The grips of the testing system were tightened firmly to avoid the slipping of the specimens. The strain rate was maintained as 1mm/min . The elongation was determined on the basis of initial specimen length and the position change of the grippers. Then, elasticity modulus was calculated on the steepest slope of the initial linear portion of the stress strain curve by using least-squares fit.

Three-point bending (flexural) tests were performed using a Zwick universal testing system per for a total of 12 times with the specimens produced parallel to XY plane, parallel to XZ plane, as-built and post-cured. The testing speed was maintained as 2mm/min . Flexural stress (strength)

and flexural modulus values were calculated by the method described in the ISO 178 standard¹⁸. First of all, flexural strength was calculated using the applied force, span length between supports, specimen width and specimen thickness. Following to that, flexural strain was also calculated using span length between supports, specimen thickness and deflection value. Finally, flexural modulus was identified using these two calculated values. The raw data that emerged as a result of the tests and calculations were collected and then graphics were generated in order to provide a clear presentation in the paper.

Charpy impact toughness tests were performed using an Instron Cease Impactor testing system per ISO 179¹⁹. Studies on the toughness of similar materials in the previous literature were taken into account, and unnotched samples were selected in order to observe the highest possible energy level²⁰. A 4 joule pendulum with an initial height of 430mm and an initial angle of 150° was used, and the values automatically calculated by the system were obtained as a result of the tests.

2.6. Microstructural characterization

Microstructural studies were carried out in order to better understand and interpret the mechanical damage of the samples and the microstructural condition causing the related damage. Microstructure investigations were carried out on tensile specimens with the lowest deformation rate and uniaxial damage to facilitate easy interpretation. Microstructure images were taken with a Carl Zeiss/Discovery V12 stereo microscope.

3. Results and Discussion

For all three specimen types, VP based AM production, subsequent post-curing and cleaning stages were completed without any problems. Figure 7 shows As-built specimens on the build platform together with together with individual photograph of each specimen.

When the dimensional measurement results are examined, it has been observed that the length, width and thickness dimensions of the specimens do not have a major difference in terms of those produced in the XY and XZ planes. However, a minor difference was detected in terms of post-curing effect. Considering the length and width values of the samples produced in different directions, it was determined that the measurement averages of the post-cured specimens were 0.17% smaller than the uncured specimens. This finding compatible with the case studies from the previous literature⁶.

Surface roughness measurements gave distinct trends between two specimen planes, especially when the measuring was direction perpendicular to the tensile testing axis. As can be seen from Figure 8, the surface texture of the specimen produced in the XY plane in a) has an average surface roughness value of $R_a\ 0.521\mu\text{m}$, while the surface texture of the sample produced in the XZ plane in b) has periodic peaks-valleys and has a value of $R_a\ 6.205\mu\text{m}$.

Surface roughness values, group averages and standard deviations are given in Table 3. The column of average group values in Table 3 clearly visualize the diverse trend of surface roughness for specimen groups which were produced at different planes and measured along different directions. In this regard,

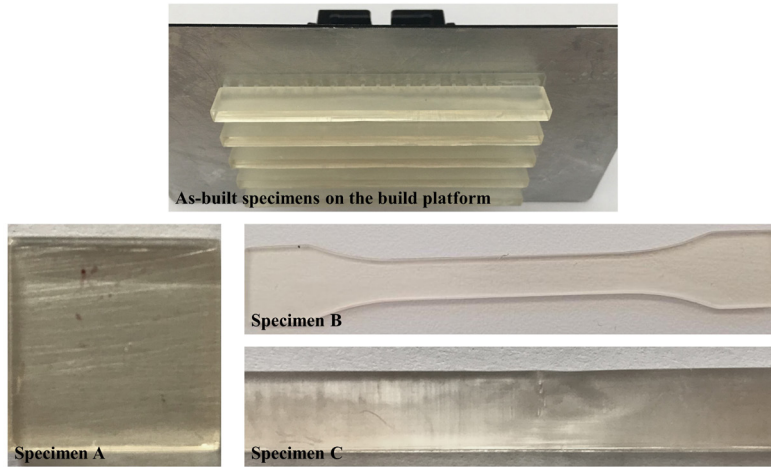


Figure 7. As-built specimens on the build platform together with together with individual photograph of each specimen.

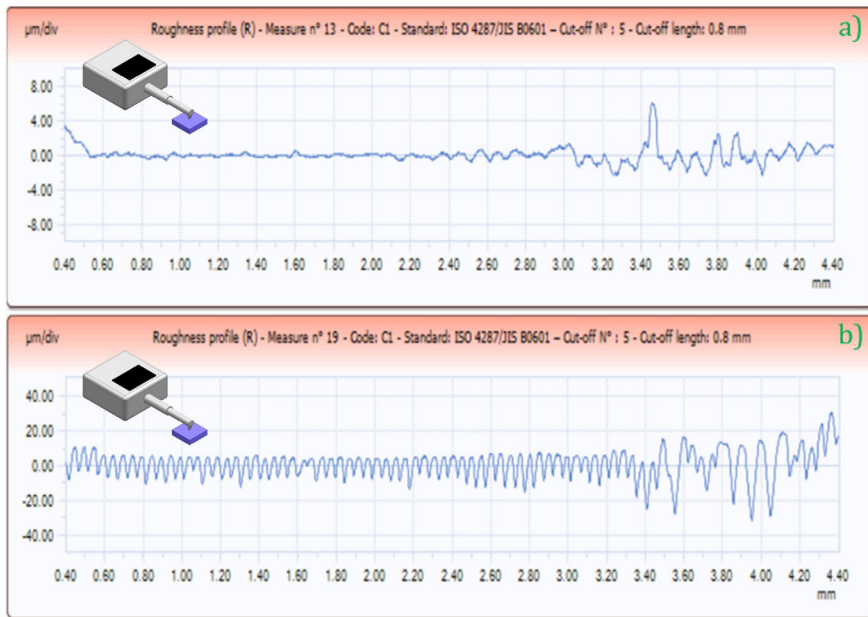


Figure 8. Roughness profiles when the measuring direction was perpendicular to the tensile testing direction: a) XY plane specimen, b) XY plane specimen.

Table 3. Surface roughness values.

| Specimen | Ra (μm) | Group average (μm) | Standard deviation (μm) |
|----------------------|----------------------|---------------------------------|--------------------------------------|
| XY_X_Parallel_1 | 0.521 | | 0.088 |
| XY_X_Parallel_2 | 0.507 | 0.646 | 0.098 |
| XY_X_Parallel_3 | 0.91 | | 0.187 |
| XY_X_Perpendicular_1 | 1.84 | | 0.243 |
| XY_X_Perpendicular_2 | 2.045 | 2.184 | 0.098 |
| XY_X_Perpendicular_3 | 2.667 | | 0.342 |
| XZ_X_Parallel_1 | 2.81 | | 0.670 |
| XZ_X_Parallel_2 | 3.87 | 3.758 | 0.079 |
| XZ_X_Parallel_3 | 4.593 | | 0.591 |
| XZ_X_Perpendicular_1 | 6.934 | | 0.424 |
| XZ_X_Perpendicular_2 | 6.046 | 6.334 | 0.203 |
| XZ_X_Perpendicular_3 | 6.021 | | 0.221 |

it can be stated that the specimens produced at XY plane have minimum surface roughness, and measurement direction difference for these specimens play a minor role. On the other hand, the specimens produced at XZ plane have rougher surface profiles and this can be associated with stair stepping effect. Stair stepping effect, which is one of the inherent and common limitations of layer-based additive manufacturing techniques, is expected to increase with increasing build direction angle and layer thickness²¹. In this study, since the layer thickness was kept constant for reaching the optimum density, the increase in the surface roughness caused by the stair stepping effect depending on the direction is in line with the previous literature²¹.

Standard deviation values are also good indicators of process capabilities and repeatability, and the surface roughness investigations conducted in this study revealed important findings. In this context, the lowest standard deviation value was found for the specimens produced in the XY plane and in the X-axis, and measured parallel to the tensile direction.

Density values that did not alter between different replicates, and they were observed as $1.207 \pm 0.001 \text{ g/cm}^3$ for as-built samples and $1.209 \pm 0.001 \text{ g/cm}^3$ for post-cured samples. The density of as-built specimens which was measured as $1.207 \pm 0.001 \text{ g/cm}^3$ is slightly lower than the density of post-cured specimens. Although the density difference between as-built and post-cured specimens is really low, approximately 0.002 g/cm^3 , it will be useful to pay attention to this result. Similar observations are reported among previous literature, and the previous researchers explained this result by relating it to shrinkage for acrylate-based resins¹⁸.

Figure 9 illustrates the FTIR spectra recorded for unprocessed raw resin (a), as-built specimens (b) and

post-cured (c) specimens. The first noteworthy features in all three of the FTIR charts are that the peaks at high wavenumber levels are in the range of $3300\text{-}3400 \text{ cm}^{-1}$ and $2900\text{-}3000 \text{ cm}^{-1}$. Among these values, especially the peak between $2900\text{-}3000 \text{ cm}^{-1}$ which indicates C-H aromatic stretch, has been reported in the past literature in ABS samples that were produced both with additive manufacturing and other conventional methods²²⁻²⁴. However, the peak observed between $3300\text{-}3400 \text{ cm}^{-1}$ at high wavenumber levels has been reported in the previous literature only in studies that produced samples with additive manufacturing^{23,24}. In addition, Mohammed et al.²⁴ stated that this peak was only seen in the specimens additively manufactured from virgin ABS material, but not in the later recycled ones²⁴.

The peaks observed around 2200 cm^{-1} in this study is also compatible with the previous literature and its value indicates $\text{C}\equiv\text{N}$ axial deformation²²⁻²⁴. However, the transmittance value of this peak is very small and this peak was seen only in as-built and post-cured samples. This result shows that the compound corresponding to the related peak appeared in the first photo-polymerization in the build phase and was not affected by post-curing. Another interpretation that can be made considering the closeness of wavenumber and transmittance values for as-built and post-cured specimen peaks in FTIR analysis results is that there is no major chemical change after the first photo-polymerization based additive manufacturing²⁵.

Thermogravimetric analysis (TGA) were conducted to comprehend the thermal stability of the specimens in as-built and post-cured conditions. The results of the analyses are presented in Figure 10. As can be seen through Figure 10 by following weight reduction and derivative weight reduction curves, the onset temperature of as-built specimens is 411.23°C while the onset temperature of post-cured specimens is 414.45°C . The onset temperature slightly above 400°C is attributed to the ABS material in the previous literature²⁶. In addition, the post-cured specimen onset temperature being

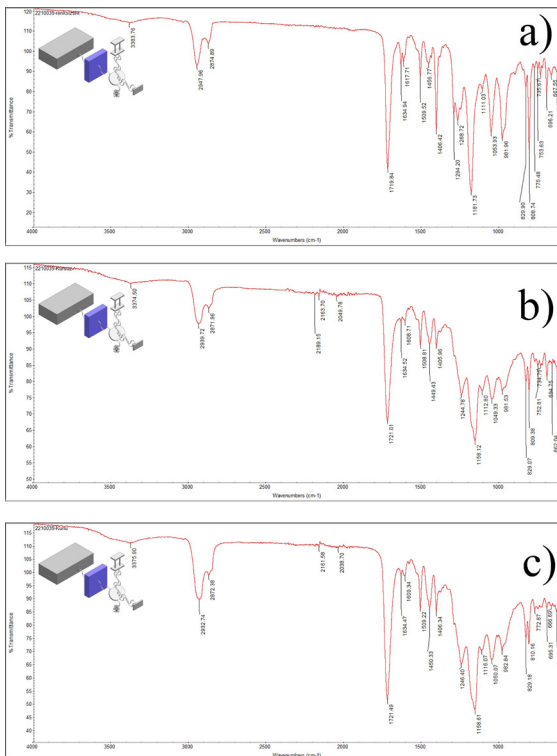


Figure 9. FTIR spectra recorded for unprocessed raw resin (a), as-built specimens (b) and post-cured specimens (c).

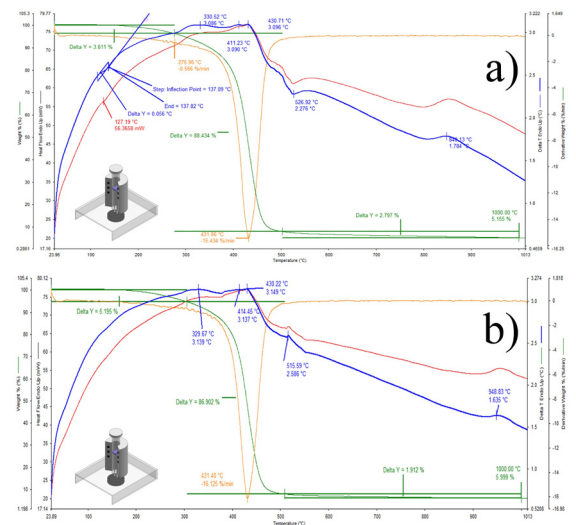


Figure 10. TGA/DTGA curves for as-built specimens (a) and post-cured specimens (b).

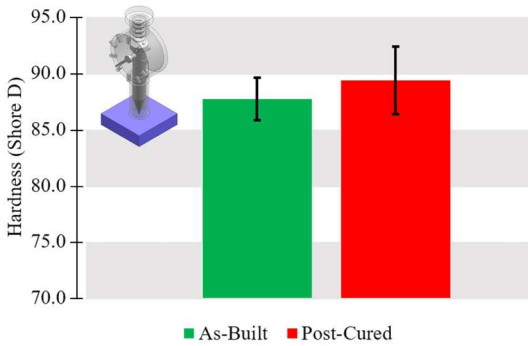


Figure 11. Shore D hardness of as-built and post-cured samples.

higher than the as-built specimen onset temperature is also in good agreement with the previous literature²⁷.

Another difference that can be observed between as-built and post-cured samples by looking at Figure 10 is the decomposition stages. Although the weight loss experienced as a result of decomposition in as-built specimens fluctuates between about 127°C and 137°C, decomposition in post-cured specimens exhibit a regular behavior. This shows the importance of the role of cross-links increasing with post-curing in the thermal stability of the material. Although DSC measurements did not give a prominent result due to the amorphous character of the specimens produced from resin, the glass transition temperature value was found to be 122°C for as-built samples and 119°C for post-cured samples.

As the initial mechanical tests, the hardness measurement results did not show a significant difference depending on the direction, similar to the density measurements. The hardness value was observed as an average of 87.7 Shore D with a standard deviation of 1.9 for the as-built samples. It was measured 89.3 Shore D average hardness with a standard deviation of 3.0 for the post-cured samples. Figure 11 shows the benchmarking of hardness values between as-built and post-cured samples. As for the hardness values which can be seen through Figure 11, it is obvious that the post-cured specimens exhibit increased results comparing to as-built specimens. This finding is also in-line with the previous literature¹².

The tensile tests were performed as described in the material and method section. Stress-elongation diagrams were plotted for the specimens subjected to tensile tests. It was observed that the stress increased continuously with elongation in the diagrams of all specimens. This relationship continued until the final damage occurred. The tensile behavior of the as-built specimen at XY plane is shown at Figure 12 as an exhibit for all the specimens having similar behaviors. In the diagram, an almost continuous relationship exists between the stress and elongation until the damage takes place.

In the tensile tests performed with 3 repetitions, the average of the stress values recorded before the damage and at the same time the standard deviation was calculated using these values. In addition, strain was obtained by proportioning the elongation values to the initial length, and the modulus of elasticity was calculated considering the regions where the stress and strain relationship is linear.

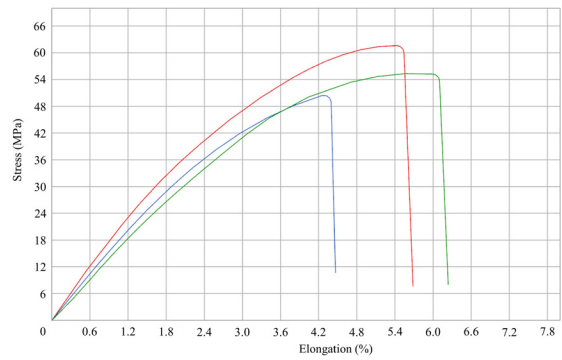


Figure 12. Stress-elongation diagram of uncured samples in XY plane.

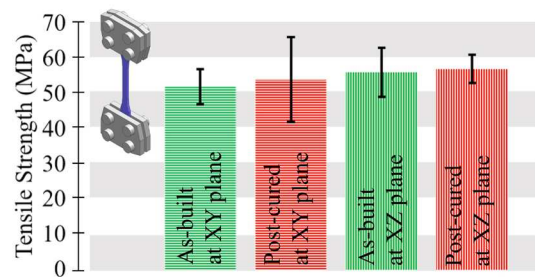


Figure 13. Tensile strength of specimens.

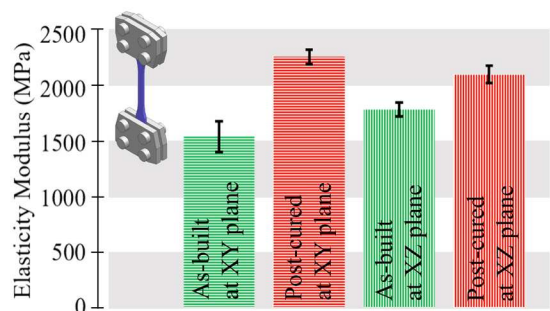


Figure 14. Elasticity modulus of specimens.

The average values and standard deviations of the stress, elasticity modulus and elongation obtained for the specimens as the result of the tests are shown in Figure 13, Figure 14 and Figure 15.

For all figures, the green columns show the test results of the as-built specimens and the red columns show the test results of the post-cured specimens. In addition, those with a horizontal line pattern are the specimens produced in the XY plane, and those with a vertical line pattern and a frame are the specimens produced in the XZ plane.

It is also believed that the hardening of specimens influences the tensile test results. By observing Figure 13 and Figure 14, it is clear that post-curing has a slight effect on tensile strength and a pronounced effect on elasticity modulus,

but the same is not true for specimen orientation. Through post-curing, tensile strength and elasticity modulus increases while elongation decreases.

Only the as-built specimens present a considerable difference depending on the specimen orientation. In this regard, specimens produced at XY plane exhibit lower elasticity modulus together with a higher elongation compared to the specimens produced at XZ plane. This finding is in line with the previous literature²⁸. In the study performed by Monzón et al.²⁹ with Visijet FTX resin, it was revealed that the modulus difference between the horizontal and vertical directions is significant only when there is no post-curing²⁹.

Still, it should be explained why the tensile strength and elasticity modulus values of as-built specimens manufactured in the XZ plane are higher than their counterparts in the

XY plane. One of the important reasons for this situation is that the exposure time during manufacturing increases the percentage of crosslinking density. In the study by Ribo²⁸, it was observed that the exposure time affected the percentage of crosslinking density for the same irradiance and energy dose used, and the mechanical properties of samples with different crosslinking density percentages altered²⁸. In another study, it was determined that increasing the exposure time increases the tensile strength value³⁰. In the present study, although the exposure time was kept constant per unit layer for all specimens, the specimens produced in the XY plane had higher number of layers than those in the XY plane, and this increased the total exposure time of the whole sample and caused a change in the mechanical properties.

In addition to tensile tests and the obtained values, the results of the micro-structural examinations of fracture surfaces performed by using a stereo microscope were also considered for better understanding of the specimens' failures. The microstructure photos of as-built and post-cured specimens manufactured at XY plane are provided in Figure 16a and Figure 16b. As an exhibit, these two figures include both the large fracture surface and the magnified view of the crack initiation region. Together with these, Figure 16c and Figure 16d just include the magnified view of the crack initiation regions of as-built and post-cured specimens manufactured at XZ plane.

As evident for the as-built specimen microstructure photos provided in Figure 16a and Figure 16c, micro-spherical voids exist before curing, and the crack initiation at those fracture

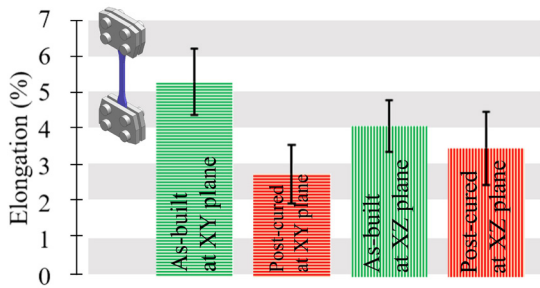


Figure 15. Elongation of specimens.

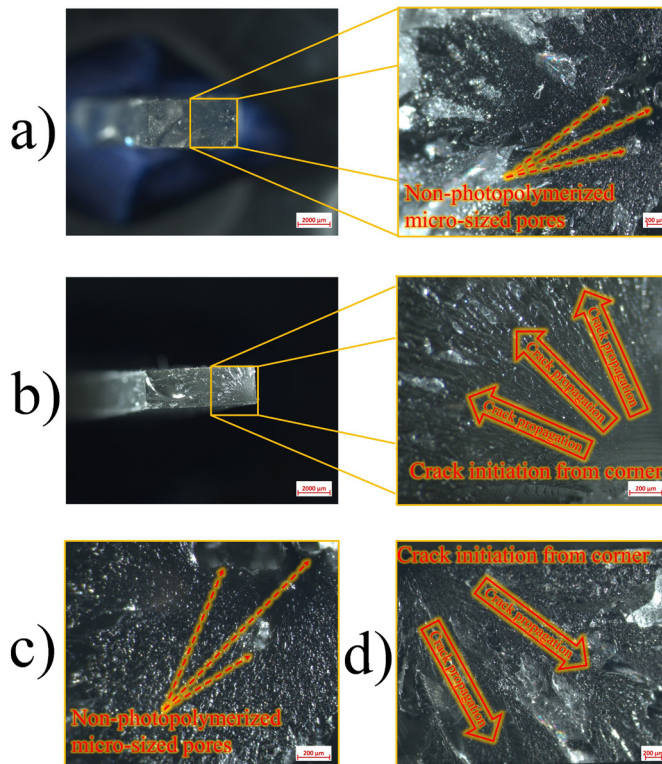


Figure 16. Microstructures of; (a) as-built specimens at XY, (b) post-cured specimens at XY, (c) as-built specimens at XZ, (d) post-cured specimens at XZ planes.

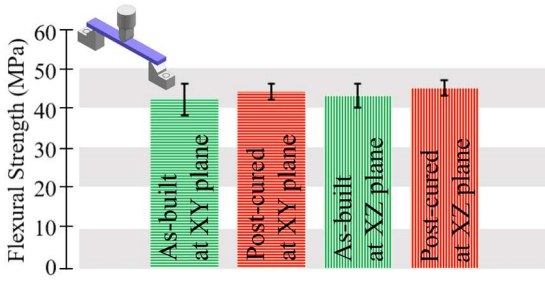


Figure 17. Flexural strength of specimens.

surfaces start from these pores or from regions close to these pores. Moreover, fracture surfaces of these specimens do not have regular crack propagation traces. On the contrary, fracture surfaces of the specimens given in Figure 16b and Figure 16d have more pronounced crack propagation traces which initiates from corners or from regions close to the corners. This finding, is inline with the previous literature, and in the microstructure investigations of successful specimens with high integrity, produced by past researchers from resin-based material, crack initiation was found in the outer corners and areas close to these³¹⁻³³. Good integrity in the internal structure of the specimens produced in this study affected the tensile strength and elasticity modules, and as a result, these two values of the post-cured specimens are higher than the as-built specimens.

It was determined that the flexural modulus and flexural strength values (Figure 17 - Figure 18) obtained as a result of three-point bending tests were slightly lower than the values obtained as a result of tensile tests for the same deformation and strain levels. This finding is consistent with the previous literature⁵. In addition, it has been revealed that the directional change in the mechanical properties representing the flexural state, similar to the tensile state, is more remarkable in as-built samples. This finding is also compatible for different resin types in the previous literature²⁹.

As for the final mechanical tests, impact resistances of the specimens are presented in Figure 19. The impact resistance of different specimens varied between 9.6-14.4kJ/m². Unfortunately, no publication has been found in the previous literature that uses exactly the same manufacturing, same sample geometry, same test conditions and same reporting methods to compare this value. For this reason, a comparison was made with the publications considered to be close to this article. In this regard, Vidakis et al.³¹, reported 16 kJ/m² impact resistance for ABS specimen which was fabricated by material extrusion based additive manufacturing³¹. In another example by Lee et al.³⁴, impact strength of denture based acrylic resin specimens fabricated by photopolymerization based AM was found to be between 8.9-14.9 kJ/m²³⁴. When these and similar close examples are examined, it is concluded that the value obtained in this study is at a reasonable level. After emphasizing the minimum and maximum impact resistance of the specimens, it would be important to benchmark the achieved values for different specimens. The maximum impact resistance is observed for as-built specimens at XZ plane while the second higher value is also achieved for as-built specimens

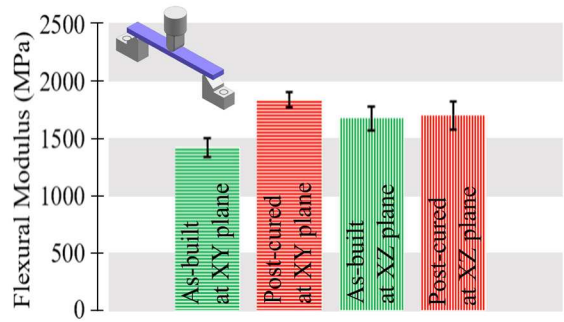


Figure 18. Flexural modulus of specimens.

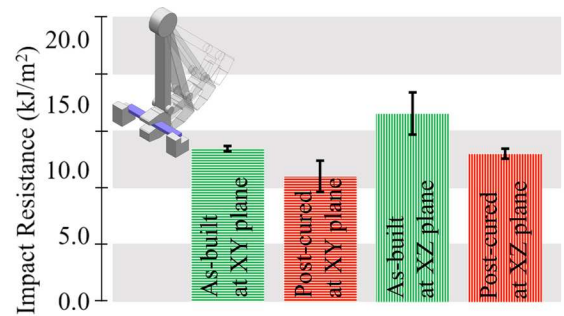


Figure 19. Impact resistance of specimens.

at XY plane. The main reason for this situation is related to the high elasticity modulus and elongation values of the as-built samples produced in both directions, as can be seen from Figure 14 and Figure 15. Specimens with high modulus absorb more energy thanks to their good elongation values after deformation in the elastic region and provide advantages in terms of toughness.

4. Conclusions

This study investigates and benchmarks the influence of build direction and post-curing on the material and part attributes of hard resins. Within the scope of this study, three types of specimens were manufactured in different build directions with the parameters that offer the highest density, and half of these specimens were also post-cured. Later on, dimensional measurements, surface roughness characterization, FTIR, TGA, DSC, hardness, tensile and impact toughness tests and analyses were performed to the specimens. The findings of the study can be summarized as follows:

- The change in the build direction significantly affects the surface roughness and the average surface roughness of the samples produced in the vertical plane is much higher than those produced in the horizontal plane.
- If the materials are post-cured after being produced with VP-based additive manufacturing, their dimensions decrease and their density increase slightly. On top of these, post-curing increases the hardness regardless of the build direction.

- Both the raw resin, as-built specimen, and post-cured specimen exhibited the characteristic ABS peak for high wavenumbers in FTIR measurements, but the peak indicating C≡N axial deformation at the wavenumber level of 2200cm⁻¹ appeared only in as-built and post-cured samples.
- TGA analyzes showed that thermal degradation of both as-built and post-cured materials started later than their conventional counterparts. Among the investigated specimens, the thermal stability of the post-cured specimen was found to be better than the as-built one.
- In addition to density and hardness, post-curing increases the tensile modulus, while decreasing the elongation.
- However, it is seen that the effect of the direction is more noticeable in the as-built samples, and it can be said that the tensile stress and elasticity modulus values for the samples produced in the XY plane are less than those produced in the XZ direction.
- Latest finding to show that as-built specimens are more resistant to impacts has been associated with greater elongation and greater energy absorption prior to failure.

5. Acknowledgements

This work, which is the part of a project named “Design, Analysis, and Verification of Triply Periodic Minimal Surface Structures by Polymer Additive Manufacturing” was financially supported by Eskişehir Technical University (ESTÜ) – Grant No: 22LÖP243. The author of the study would like to acknowledge BTU MERLAB, ESOGU ARUM and TUBITAK MAM for providing the test services.

6. References

1. Li N, Huang S, Zhang G, Qin R, Liu W, Xiong H et al. Progress in additive manufacturing on new materials: a review. *J Mater Sci Technol.* 2019;35(2):242-69.
2. Martínez-García A, Monzón M, Paz R. Standards for additive manufacturing technologies: structure and impact. In: Antonio Riveiro JP, Davim JP, editors. *Additive manufacturing.* Amsterdam: Elsevier; 2021. p. 395-408.
3. Kushan MC, Poyraz O, Uzunonat Y, Orak S. Systematical review on the numerical simulations of laser powder bed additive manufacturing. *Sigma J Eng Nat Sci.* 2018;36(4):1195-212.
4. Wohlers T, Gornet T. History of additive manufacturing [Internet]. Fort Collins: Wohlers Associates, Inc; 2015 [cited 2022 Jun 13]. 35 p. Available from: <https://wohlersassociates.com/wp-content/uploads/2022/08/history2015.pdf>
5. Pagac M, Hajnys J, Ma QP, Jancar L, Jansa J, Stefek P et al. A review of vat photopolymerization technology: materials, applications, challenges, and future trends of 3D printing. *Polymers.* 2021;13(4):1-20.
6. Kiliç V, Camadanlı Ş. The effect of triacrylate monomer structure on volume shrinkage and tensile properties of vat polymerization resins. *Int J 3D Print Technol Digit Ind.* 2021;5(2):220-6.
7. Lee JY, An J, Chua CK. Fundamentals and applications of 3D printing for novel materials. *Appl Mater Today.* 2017;7:120-33.
8. Sycks DG, Wu T, Park HS, Gall K. Tough, stable spiroacetal thiolene resin for 3D printing. *J Appl Polym Sci.* 2018;135(22):46259.
9. Borrello J, Nasser P, Iatridis JC, Costa KD. 3D printing a mechanically-tunable acrylate resin on a commercial DLP-SLA printer. *Addit Manuf.* 2018;23:374-80.
10. Schmidleithner C, Kalaskar DM. Stereolithography. In: Cvetković D, editor. *3D printing.* London: IntechOpen; 2018. p. 1-22.
11. Hu R, Huang B, Xue Z, Li Q, Xia T, Zhang W et al. Synthesis of photocurable cellulose acetate butyrate resin for continuous liquid interface production of three-dimensional objects with excellent mechanical and chemical-resistant properties. *Carbohydr Polym.* 2019;207:609-18.
12. Dizon JRC, Espera AH Jr, Chen Q, Advincula RC. Mechanical characterization of 3D-printed polymers. *Addit Manuf.* 2018;20:44-67.
13. Jafferson JM, Chatterjee D. A review on polymeric materials in additive manufacturing. *Mater Today Proc.* 2021;46:1349-65.
14. Carolo L, Obudho B [homepage on the Internet]. Munich: All3DP; c2021 [cited 2022 Jun 14]. Available from: <https://all3dp.com/2/best-tough-resin-abs-like-resin/>
15. Wang Y, Li X, Chen Y, Zhang C. Strain rate dependent mechanical properties of 3D printed polymer materials using the DLP technique. *Addit Manuf.* 2021;47:102368.
16. Markiz N, Horváth E, Ficzero P. Influence of printing direction on 3D printed ABS specimens. *Prod Eng Arch.* 2020;26(3):127-30.
17. Dokuz Kimya [homepage on the Internet]. Aydın: Dokuz Kimya; c2023 [cited 2022 Jun 14]. Available from: <https://www.dokuzkimya.com/products/alias-model-recinesi-beyaz?variant=41108226179267>
18. ISO: International Organization for Standardization. ISO 178:2010—plastics—determination of flexural properties. Geneva: ISO; 2010.
19. ISO: International Organization for Standardization. ISO 179-1: plastics: determination of Charpy impact properties. Part 1: non-instrumented impact test. Geneva: ISO; 2000.
20. Vidakis N, Petousis M, Vairis A, Savvakis K, Maniadi A. A parametric determination of bending and Charpy's impact strength of ABS and ABS-plus fused deposition modeling specimens. *Prog Addit Manuf.* 2019;4(3):323-30.
21. Poyraz Ö, Solakoğlu EU, Soner Ö, Tüzemen C, Akbulut G. Surface texture and form characterization for powder bed additive manufacturing. *J Fac Eng Archit Gazi Univ.* 2019;34(3):1653-64.
22. Ferreira AC, Diniz MF, Mattos EDC. FT-IR methodology (transmission and UATR) to quantify automotive systems. *Polímeros.* 2018;28(1):6-14.
23. Zhang SU. Degradation classification of 3D printing thermoplastics using Fourier transform infrared spectroscopy and artificial neural networks. *Appl Sci.* 2018;8(8):1224.
24. Mohammed MI, Wilson D, Gomez-Kervin E, Tang B, Wang J. Investigation of closed-loop manufacturing with acrylonitrile butadiene styrene over multiple generations using additive manufacturing. *ACS Sustain Chem & Eng.* 2019;7(16):13955-69.
25. Voet VS, Strating T, Schnelting GH, Dijkstra P, Tietema M, Xu J et al. Biobased acrylate photocurable resin formulation for stereolithography 3D printing. *ACS Omega.* 2018;3(2):1403-8.
26. Capote GAM, Montoya-Ospina MC, Liu Z, Mattei MS, Liu B, Delgado AP et al. Compounding a high dielectric constant thermoplastic material for production of microwave photonic crystals through additive manufacturing. *ChemRxiv.* 2021 [cited 2023 Mar 1];1-16. <https://chemrxiv.org/engage/chemrxiv/article-details/61a538b7568d3365e34b3c61>.
27. Zirak N, Shirinbayan M, Benfriha K, Deligant M, Tcharkhtchi A. Stereolithography of (meth) acrylate-based photocurable resin: thermal and mechanical properties. *J Appl Polym Sci.* 2022;139(22):52248.
28. Ribo MM. Vat photopolymerization process chain [PhD thesis]. Lyngby: Denmark Technical University; 2020.

29. Monzón M, Ortega Z, Hernández A, Paz R, Ortega F. Anisotropy of photopolymer parts made by digital light processing. *Materials*. 2017;10(1):64.
30. Lovo JFP, Camargo ILD, Erbereli R, Morais MM, Fortulan CA. Vat photopolymerization additive manufacturing resins: analysis and case study. *Mater Res*. 2020;23(4):e20200010.
31. Vidakis N, Petousis M, Michailidis N, Kechagias JD, Mountakis N, Argyros A et al. High-performance medical-grade resin radically reinforced with cellulose nanofibers for 3D printing. *J Mech Behav Biomed Mater*. 2022;134:105408.
32. Wang Y, Li X, Chen Y, Zhang C. Strain rate dependent mechanical properties of 3D printed polymer materials using the DLP technique. *Addit Manuf*. 2021;47:102368.
33. Hua W, Lin Q, Qu B, Zheng Y, Liu X, Li W et al. Exceptional mechanical properties and heat resistance of photocurable bismaleimide ink for 3D printing. *Materials*. 2021;14(7):1708.
34. Lee J, Belles MD, Gonzalez M, Kiat-Amnuay S, Dugarte A, Ontiveros MJ. Impact strength of 3D-printed and conventional heat-cure and cold-cure denture base acrylic resins. *Int J Prosthodont*. 2022;35(2):240-4.